^{68}Ga-DOTA-Tyr^3-Octreotide PET in Neuroendocrine Tumors: Comparison with Somatostatin Receptor Scintigraphy and CT

Michael Gabriel[1], Clemens Decristoforo[1], Dorota Kendler[1], Georg Dobrozemsky[1], Dirk Heute[1], Christian Uprimny[1], Peter Kovacs[2], Elisabeth Von Guggenberg[1], Reto Bale[2], and Irene J. Virgolini[1]

[1]*Department of Nuclear Medicine, Innsbruck Medical University, Innsbruck, Austria; and* [2]*Division of Diagnostic Radiology I, Department of Diagnostic Radiology, Innsbruck Medical University, Innsbruck, Austria*

The aim of this study was to evaluate the diagnostic value of a new somatostatin analog, ^{68}Ga-labeled 1,4,7,10-tetraazacyclododecane-*N,N′,N″,N‴*-tetraacetic acid-D-Phe^1-Tyr^3-octreotide (^{68}Ga-DOTA-TOC), for PET in patients with known or suspected neuroendocrine tumors. PET was compared with conventional scintigraphy and dedicated CT. **Methods:** Eighty-four patients (48 men, 36 women; age range, 28–79 y; mean age ± SD, 58.2 ± 12.2 y) were prospectively studied. For analysis, patients were divided into 3 groups: detection of unknown primary tumor in the presence of clinical or biochemical suspicion of neuroendocrine malignancy (n = 13 patients), initial tumor staging (n = 36 patients), and follow-up after therapy (n = 35 patients). Each patient received 100–150 MBq ^{68}Ga-DOTA-TOC. Imaging results of PET were compared with ^{99m}Tc-labeled hydrazinonicotinyl-Tyr^3-octreotide (^{99m}Tc-HYNIC-TOC) and ^{111}In-DOTA-TOC. CT was also performed on every patient using a multidetector scanner. Each imaging modality was interpreted separately by observers who were unaware of imaging findings before comparison with PET. The gold standard for defining true-positive (TP), true-negative (TN), false-positive (FP), and false-negative (FN) results was based on all available histologic, imaging, and follow-up findings. **Results:** PET was TP in 69 patients, TN in 12 patients, FP in 1 patient, and FN in 2 patients, indicating a sensitivity of 97%, a specificity of 92%, and an accuracy of 96%. The FP finding was caused by enhanced tracer accumulation in the pancreatic head, and the FN results were obtained in patients with a tumor of the gastrointestinal tract displaying liver metastases. ^{68}Ga-DOTA-TOC showed higher diagnostic efficacy compared with SPECT (TP in 37 patients, TN in 12 patients, FP in 1 patient, and FN in 34 patients) and diagnostic CT (TP in 41 patients, TN in 12 patients, FP in 5 patients, and FN in 26 patients). This difference was of statistical significance ($P < 0.001$). However, the combined use of PET and CT showed the highest overall accuracy. **Conclusion:** ^{68}Ga-DOTA-TOC PET shows a significantly higher detection rate compared with conventional somatostatin receptor scintigraphy and diagnostic CT with clinical impact in a considerable number of patients.

Received Aug. 13, 2006; revision accepted Nov. 2, 2006.

For correspondence or reprints contact: Michael Gabriel, MD, Department of Nuclear Medicine, Innsbruck Medical University, Anichstrasse 35, 6020 Innsbruck, Austria.

E-mail: michael.gabriel@i-med.ac.at

Key Words: ^{68}Ga; PET; DOTA-Tyr^3-octreotide; neuroendocrine tumors; somatostatin receptor scintigraphy; diagnostic CT

J Nucl Med 2007; 48:508–518

DOI: 10.2967/jnumed.106.035667

Neuroendocrine tumors (NET) are a heterogeneous group of neoplasms that originate from the neural crest. These tumors are characterized by their ability to overexpress somatostatin (SST) receptors in most cells deriving from so-called neuroendocrine dispersed cells (*1*). The main primary sites are the gastrointestinal tract and the lung (*2,3*), but NET can also originate from various other sites, such as the head and neck region or the prostate.

Scintigraphy with radiolabeled SST analogs, first with an ^{123}I label (*4*) and subsequently with an ^{111}In (*4,5*) and ^{99m}Tc label (*6*), has proven useful in diagnosing these tumors. This method also shows the content of SST receptors that might indicate efficacy for treatment with octreotide or other SST analogs (*1*). Although SST receptor scintigraphy (SRS) shows high efficacy for whole-body imaging, there are some limitations in organs with higher physiologic uptake—for example, liver (*7,8*)—and in terms of detection of smaller lesions due to the detection limits of SPECT for the mentioned radiotracers. ^{18}F-FDG PET scanning is another widely accepted imaging approach in clinical oncology. Although ^{18}F-FDG PET shows high spatial resolution, unlike for many other malignancies, it is not indicated primarily for NET because of its poor sensitivity to detect tumors with low metabolic activity and slow growth (*9*).

On the other hand, morphologically orientated imaging techniques, such as contrast-enhanced multidetector CT, permit rapid volumetric acquisition and dynamic analysis of the contrast agent, which provides higher image resolution and gives information about the vascular phase for detection of even small-sized lesions of neuroendocrine origin (*10*). However, these methods sometimes lack specificity, as conclusions regarding malignant involvement of

organ structures are based only on size criteria and the contrast enhancement pattern (*11*).

Initial patient studies have demonstrated the capability of PET technology using ^{68}Ga-labeled 1,4,7,10-tetraazacyclododecane-*N,N′,N″,N‴*-tetraacetic acid-D-Phe^1-Tyr^3-octreotide (^{68}Ga-DOTA-TOC) (*12,13*). This method clearly offers higher resolution and improved pharmacokinetcs compared with SRS, with promising results in the detection of SST receptor-expressing tumors.

The aim of the present study was to provide data on diagnostic efficacy of the new radiopharmaceutical ^{68}Ga-DOTA-TOC for PET in a larger series of patients with known or suspected NET. The study included comparison with SPECT and CT. Patient and site-related differences of the 3 imaging modalities were analyzed in a head-to-head comparison by means of image fusion.

MATERIALS AND METHODS

Patients

From September 2004 to April 2006, 84 consecutive patients (48 men, 36 women; age range, 28–79 y; mean age ± SD, 58.2 ± 12.2 y) were enrolled in this prospective phase IIb study. For analysis, the patients who were investigated were divided into 3 groups (*14*): The first group consisted of patients who underwent imaging for the initial detection and localization of suspected NET and potential metastases in the presence of clinical or biochemical suspicion (detection; $n = 13$). Patients with histologically proven neuroendocrine malignancies were enrolled for staging purposes in the second group (staging; $n = 36$). In the third group, patients were referred during posttherapy follow-up (follow-up; $n = 35$) to exclude or to detect tumor recurrence. In the last 2 groups, at least 1 tumor manifestation was histologically confirmed in patients with multiple metastases. The patient characteristics are summarized in Table 1.

Four patients had hypoglycemia with symptoms of both neuroglycopenia and catecholamine response. During symptoms, blood glucose levels were <40 mg/dL. Therefore, a pancreatic islet cell tumor was considered in these patients.

NET are generally differentiated between those producing hormone-related symptoms (e.g., flush or diarrhea) and those presenting without any hormonal symptoms. Accordingly, 27 patients with clinical and biochemical signs for a secreting tumor and 57 patients with a nonfunctional tumor were included.

In patients who were referred for restaging during follow-up ($n = 35$), various therapeutic procedures were performed before inclusion. Most of these patients were treated by surgery ($n = 29$), some of them without further treatment ($n = 6$). Additional drug therapy was administered to 23 patients. Seven patients were treated with chemotherapy, and 16 patients were treated with long-acting SST analogs alone or in combination with interferon-α.

Written informed consent was obtained from all patients before being included in the study, and the study was approved by the local ethics committee.

PET

Preparation of ^{68}Ga-DOTA-TOC. ^{68}Ga-DOTA-TOC was prepared using a modification of the method described by Breeman et al. (*15*). Briefly, a TiO_2-based commercially available ^{68}Ge/^{68}Ga generator (Cyclotron Inc.) was eluted with 0.1N hydrochloric acid, and a 1.2-mL fraction was added to 20–40 μg of DOTA-TOC; pH was adjusted to 3.5–4.0 by adding 1 mol/L sodium acetate solution, which was followed by heating to 100°C for 7 min. The reaction solution was passed over a C_{18} cartridge (Sep-Pak; Waters), washed with 4 mL of water, and finally eluted with 0.5 mL 95% ethanol, which was followed by saline through a 0.2-μm sterile filter. Radiochemical purity, as determined by instant thin-layer chromatography and high-performance liquid chromatography, exceeded 95% in all cases.

Data Acquisition and Processing. Data acquisition was performed by means of a dedicated PET scanner (GE Advance) with 15-cm axial field of view (FOV) and 55-cm transaxial FOV. Patients were imaged in 2-dimensional mode using septa. the duration of acquisition was 5 min per bed position (axial FOV) in emission mode. For the evaluation of the best imaging time, 3 emission image sets were acquired at 20, 60, and 100 min after injection. Because of scan time limitations, the first and last acquisitions scanned only the torso (4 bed positions), whereas the acquisition at 1 h after injection was performed as a whole-body scan (from head to middle of the upper leg, usually 7 bed positions). Attenuation correction was performed by means of transmission data (^{68}Ga pin source, 3 min per bed position). Image reconstruction was performed with the system's implementation of the ordered-subsets expectation maximization iterative algorithm, using segmented attenuation correction and model-based scatter correction. The settings for iterative reconstruction were 2 iterations and 26 subsets, with 4-mm full width at half maximum (FWHM) interupdate filtering and 6-mm FWHM after filtering. The attenuation correction settings were set to segmented correction with 10-mm smoothing. No axial smoothing was performed for either emission or transmission data. For the first 8 patients, average tissue standardized uptake values (SUVs) (SUV_{bw}, units of g/mL; bw indicates body weight) have been determined by means of manually drawn regions of interest delineating the respective tissue thresholded to 50% of the maximum uptake in that tissue.

SRS

^{99m}Tc-Labeled hydrazinonicotinyl-Tyr^3-octreotide (^{99m}Tc-HYNIC-TOC) was prepared using a kit formulation as recently described (*16*). Each patient received a mean activity of 400 MBq (intravenously) of the tracer. Whole-body imaging was performed at 2 and 4 h after injection using a dual-detector VertexPlus scintillation camera (Philips), which was followed by SPECT (6). The scan speed for whole-body imaging was 10 cm/min when using the ^{99m}Tc-labeled derivative. The camera was equipped with a low-energy, all-purpose, parallel-hole collimator (window setting, 140 keV; width, 10%; 180° rotation detector head; 64 projections; 128 × 128 matrix; 40-s acquisition time per projection). The SPECT image data were reconstructed by standard filtered backprojection using a Butterworth filter.

DOTA-TOC was radiolabeled as reported elsewhere (*17*). ^{111}In-DOTA-TOC whole-body scintigraphy in anterior and posterior views was performed at 4, 24, and 48 h after a single-dose injection of 150 MBq of the ^{111}In-labeled radiopharmaceutical. Scintigraphic acquisitions were obtained with the same double-head γ-camera as described (ADAC; VertexPlus), equipped with a medium-energy, parallel-hole collimator (window setting, 172 and 246 keV; window width, 20%). The scan speed for whole-body imaging was 5 cm/min using the ^{111}In-labeled radiopharmaceutical.

TABLE 1
Patient Characteristics

Patient no.	Sex	Age (y)	Pathology	Indication	Clinical symptoms*	Confirmation†
1	M	49	Paraganglioma	Follow-up	No	Histology
2	F	57	Carcinoid of pancreas	Follow-up	No	CT
3	F	47	Carcinoid of pancreas	Follow-up	Diarrhea	CT
4	M	59	Carcinoid of pancreas	Follow-up	No	CT
5	M	79	Carcinoid of pancreas	Follow-up	No	CT
6	M	48	Carcinoid of pancreas	Follow-up	No	CT
7	M	61	Broncogenic carcinoid	Follow-up	No	CT, NaF
8	M	59	Small bowel carcinoid (gastrinoma)	Staging	Gastritis	CT
9	M	62	Small bowel carcinoid	Staging	Flush	CT, MRI
10	F	66	Small bowel carcinoid	Staging	Diarrhea	CT
11	M	39	Elevation of CgA and NSE	Detection	No	CT, MRI
12	F	28	Elevation of ACTH	Detection	Cushing	Histology, CT
13	F	62	Carcinoid of pancreas	Staging	Flush	Histology, CT
14	F	75	NET unknown primary	Follow-up	No	CT
15	M	45	Carcinoid of pancreas	Staging	Diarrhea	CT
16	F	50	NET unknown primary	Follow-up	No	CT
17	F	70	Carcinoid of pancreas	Follow-up	Diarrhea	CT
18	F	61	Elevation of CgA and NSE	Detection	No	Histology
19	F	68	NET unknown primary (gastrinoma)	Staging	Flush	CT
20	M	55	Small bowel carcinoid	Follow-up	No	CT, MRI
21	F	40	NET of hypophysis	Staging	No	MRI
22	M	61	NET unknown primary	Staging	No	MRI, NaF
23	M	61	Carcinoid of pancreas	Staging	No	CT
24	F	54	Carcinoid of pancreas	Follow-up	No	CT
25	M	55	Carcinoid of pancreas (gastrinoma)	Staging	Gastritis	CT
26	F	64	NET unknown primary	Staging	No	CT
27	F	56	NET unknown primary	Follow-up	No	CT, MRI
28	F	57	Hypoglycemia	Detection	NGP and CCR	Histology
29	F	41	Carcinoid of pancreas	Staging	No	CT
30	M	73	Elevation of CgA and NSE	Detection	Diarrhea	MRI, histology
31	M	75	Hypoglycemia	Detection	NGP and CCR	MRI
32	M	51	Carcinoid of stomach	Staging	No	CT
33	F	58	NET unknown primary	Follow-up	Flush, diarrhea	CT
34	M	63	Elevation of CgA and NSE	Detection	Diarrhea	CT, MRI
35	M	62	Small bowel carcinoid	Staging	No	CT
36	F	47	NET unknown primary	Staging	No	CT, histology
37	F	28	Elevation of CgA and NSE	Detection	No	Histology
38	F	41	Broncogenic carcinoid	Follow-up	No	CT
39	M	51	Carcinoid of pancreas	Staging	Diarrhea	CT
40	F	40	Elevation of CgA and NSE	Detection	No	Histology
41	M	77	NET of prostate gland	Staging	No	CT, NaF
42	M	54	Hypoglycemia	Detection	NGP and CCR	CT, MRI
43	M	69	Carcinoid of stomach	Staging	No	CT
44	M	64	Carcinoid of pancreas	Staging	No	CT
45	M	84	Carcinoid of pancreas	Staging	Flush	CT, MRI
46	M	74	NET unknown primary	Staging	No	CT
47	M	74	Broncogenic carcinoid	Staging	No	CT
48	F	43	Carcinoid of pancreas	Staging	No	CT, MRI
49	M	56	Small bowel carcinoid	Staging	No	CT
50	F	57	Small bowel carcinoid	Staging	No	CT, NaF
51	F	58	Small bowel carcinoid	Staging	Flush	CT
52	M	55	Elevation of CgA and NSE	Detection	No	Histology
53	F	51	Elevation of gastrin	Detection	Gastritis	CT, MRI, biopsy
54	M	62	Broncogenic carcinoid	Follow-up	No	CT, MRI
55	M	40	Carcinoid of pancreas (VIPoma)	Staging	Diarrhea	CT, NaF
56	F	67	Small bowel carcinoid	Follow-up	No	CT
57	F	76	Carcinoid of stomach	Staging	Diarrhea	CT, NaF
58	M	34	Carcinoid of pancreas	Follow-up	No	CT, NaF
59	M	66	Small bowel carcinoid	Staging	No	CT
60	M	64	Small bowel carcinoid	Follow-up	No	CT
61	M	58	Small bowel carcinoid	Follow-up	Flush, diarrhea	CT

TABLE 1
(Continued)

Patient no.	Sex	Age (y)	Pathology	Indication	Clinical symptoms*	Confirmation†
62	M	59	Small bowel carcinoid	Staging	No	CT
63	F	75	Small bowel carcinoid	Staging	No	CT, MRI
64	M	47	Small bowel carcinoid	Follow-up	No	CT
65	F	61	Broncogenic carcinoid	Follow-up	No	CT, MRI
66	M	62	Small bowel carcinoid	Staging	No	CT
67	M	35	Carcinoid of middle ear	Follow-up	No	CT, MRI
68	M	65	Carcinoid of cecum	Follow-up	Flush	CT
69	M	62	Small bowel carcinoid	Follow-up	Diarrhea	CT
70	M	50	Small bowel carcinoid	Staging	No	CT
71	F	78	Small bowel carcinoid	Follow-up	No	CT, NaF
72	F	37	Hypoglycemia	Detection	NGP and CCR	CT, MRI
73	M	73	Paraganglioma	Follow-up	No	CT, MRI
74	M	79	Carcinoid of rectum	Staging	No	CT
75	F	64	Carcinoid of stomach	Follow-up	No	CT
76	F	66	Broncogenic carcinoid	Follow-up	No	CT
77	F	60	Small bowel carcinoid	Follow-up	Diarrhea	CT
78	M	67	Carcinoid of rectum	Follow-up	No	CT
79	M	69	Paraganglioma	Staging	No	MRI, histology
80	F	47	Small bowel carcinoid	Follow-up	No	CT, MRI, histology
81	F	59	Carcinoid of pancreas	Follow-up	No	CT, NaF
82	M	59	Carcinoid of pancreas	Staging	No	CT, MRI, NaF
83	M	65	Small bowel carcinoid	Follow-up	No	CT
84	M	54	Small bowel carcinoid	Follow-up	No	CT

*NGP and CCR = symptoms of neuroglycopenia and catecholamine response.
†NaF = ^{18}F-Na-fluoride PET.
CgA = chromogranin A; NSE = neuron-specific enolase; ACTH = adrenocorticotropic hormone; VIPoma = vasoactive intestinal peptide-producing tumor.

SPECT was acquired after 24-h whole-body imaging using the same reconstruction algorithm as mentioned earlier.

Sixty-six patients were investigated with only 1 tracer: 33 patients with ^{99m}Tc-HYNIC-TOC and 33 with ^{111}In-DOTA-TOC. In 18 patients, both radiopharmaceuticals were used for comparison with PET and CT.

CT and Image Fusion Procedure

Helical CT scans of the thorax and the abdomen with a slice thickness of 2.5 mm were obtained with the HiSpeed CT/i Advantage scanner (GE Healthcare). Typically, 150 mL (twice the weight of the patient in kilograms) iopromidum contrast media (Ultravist 370; Schering) were administered at 5 mL/s, with scan delays of approximately 30 s for the late arterial phase and 70 s for the portal phase.

For image fusion, the PET, SPECT, and CT scans were performed sequentially using an individualized vacuum mattress with external markers attached to it. For every image acquisition (PET, SPECT, and CT), the patient was repositioned into the vacuum mattress (*11*). The image fusion procedure was used for anatomic delineation of abnormal findings in SPECT and PET.

Interpretation and Data Evaluation

PET and SPECT studies were interpreted independently by 2 experienced nuclear medicine physicians. Corresponding studies were compared lesion by lesion for final analysis and ruled as matching or mismatching by the 2 nuclear medicine specialists. If the result of the 2 viewers was discordant, a third reader—who acted as referee—was consulted. They were aware of the patients' clinical history, which was provided by the referring physician but were unaware of any result of other imaging modalities. The criteria for image interpretation of PET and SPECT are summarized in Table 2. As a measure for diagnostic yield, the number of lesions that could be identified clearly as single foci was determined. Lesions within the liver were rated as 1 organ metastasis, considering the irregular configuration and confluence of some lesions, so that an individual metastasis frequently was not delineated. A lesion-by-lesion analysis was performed for all other tumor foci. Concordant findings on nuclear medicine techniques (PET and SPECT) and CT meant that both techniques (PET or SPECT and CT) were consistent with malignancy. In the case of discrepancies with regard to nuclear medicine and CT findings, further assessment of abnormal foci was mandatory—that is, by histologic proof or follow-up controls with CT or MRI after 3 mo and, if necessary, after 6 mo. If malignant evolution on follow-up or progression on therapy was observed, these suggestive findings were considered malignant for the final decision. Those patients with no abnormal findings were monitored over a period of at least 6 mo with repeated CT or MR scans before a scan result was considered true-negative (TN).

CT and, if necessary, MR scans were interpreted by experienced radiologists who were unaware of the scintigraphic results. A positive diagnosis was based on the specific appearance of malignant disease derived from NET as reported elsewhere (*18*). Thus far, abnormal findings were assessed histologically in 13 patients. Repeated clinical examinations with CT were performed

TABLE 2
Criteria for Visual Study Interpretation

Uptake	Features of tracer accumulation
Nonmalignant	Linear, nonfocal limited intestinal uptake with moderate intensity
	Tracer uptake less intense than liver uptake
	Pancreatic head (PET): small sickle-shaped findings in right upper abdomen just below left liver lobe; diffuse nature of uptake
Malignant	Clearly demarked findings with higher tracer uptake compared with liver uptake
	Tracer accumulation in structures that did not take up tracer physiologically or was higher than background activity
	Pancreatic head: irregular or protrusive shape of finding; clear delineation from adjacent tissue with higher uptake than liver uptake

in 73 cases and with MR in 22 cases. More details are given in Table 1. Attention has been directed toward unproven findings of the scans.

Statistical Analysis

The results of the 3 imaging modalities (PET, SPECT, and CT) were classified as true-positive (TP), TN, false-positive (FP), or false-negative (FN) according to the reference standard, as described earlier. The χ^2 test for independence, or the Fisher exact test when appropriate, was used to evaluate differences in lesion detectability when subgroups of the patients being investigated were statistically compared (^{111}In-DOTA-TOC vs. ^{99m}Tc-HYNIC-TOC and secreting vs. nonsecreting tumors). The McNemar test of correlated properties was used to statistically compare the imaging results of ^{68}Ga-DOTA-TOC PET with SPECT and diagnostic CT. Analysis was done on a lesion basis and on a patient basis. All P values < 0.05 were considered significant. Cohen's κ-statistic with 95% confidence intervals was calculated to show the degree of association between the techniques. The function of uptake over time was assessed using linear regression analysis.

For evaluation of the clinical value of ^{68}Ga-DOTA-TOC PET in comparison with the other imaging modalities, organ systems were assessed for recognition of any lesion in the tissue. The focus of interest was related to unknown tumor lesions arising in organ systems, unaware of malignant involvement from other imaging techniques (e.g., bone), with clinically relevant information in terms of further patient management.

RESULTS

Biodistribution of ^{68}Ga-DOTA-TOC

Uptake of ^{68}Ga-DOTA-TOC was routinely found in neuroendocrine tissue (pituitary and adrenal glands) and in 57 patients (67.8%) in the pancreatic head without known pathology. Additionally, the spleen and the urinary excretion system also showed enhanced tracer accumulation. Homogeneous uptake was observed in the liver and in 34 patients (40.4%) in the thyroid gland. Because of the excellent tumor-to-organ contrast, NET lesions could be easily identified by visual analysis (Fig. 1). However, anatomic delineation of abnormal findings was difficult without image fusion because of highly specific tracer uptake. Intravenous injection of ^{68}Ga-DOTA-TOC was well tolerated in all patients, and no side effects were observed in any patients after tracer injection. On the basis of an initial evaluation of 8 patients, the optimal time of acquisition was determined to be 100 min after injection. In 1 of these 8 patients, 2 additional thoracic findings were observed when comparing late acquisition 100 min after injection with the earlier acquisition (patient 12). The acquisition protocol was adapted after this initial series with only 1 single whole-body scanning at 100 min after injection. Linear regression analysis of tumor uptake values shows a significant increase in SUVs of 14% (60 min vs. 20 min, $R^2 = 0.96$), 9% (100 vs. 60 min, $R^2 = 0.97$), and 24% (100 vs. 20 min, $R^2 = 0.89$). Interpatient SUVs at different times are given in Table 3.

Analysis on Patient Basis

Results from all 84 patients studied are summarized in Table 4. Among the 84 patients, ^{68}Ga-DOTA-TOC PET was TP in 69 (82.1%), TN in 12 (14.3%), FP in 1 (1.2%), and FN in 2 (2.4%) patients, indicating a sensitivity of 97% (69/71 patients), a specificity of 92% (12/13 patients), and an accuracy of 96% (81/84 patients) on a patient basis. An analysis per patient comparing the scan results of PET with SPECT and with diagnostic CT emphasizes the improved diagnostic efficacy of ^{68}Ga-DOTA-TOC, with a P value of < 0.001 using the McNemar test (Table 5). Cohen's κ-statistic of 0.3 showed only fair association between the techniques.

Analysis on Lesion Basis

^{68}Ga-DOTA-TOC PET studies detected 375 abnormal findings in 70 patients, of which 374 were TP and 1 was FP. This FP finding was found in patient 30, who had clinical symptoms suggestive of a secreting NET and elevated tumor markers (chromogranin A [CgA] of 34.6 U/L and neuron-specific enolase [NSE] of 26.7 μg/L) and who presented with enhanced tracer uptake in the pancreatic head. Surgical exploration was negative, and histology and further follow-up controls did not confirm this finding to be malignant. Overall, 23 abnormal findings in 22 patients were considered malignant in the pancreas. Fourteen of those were found in the pancreatic head, with 1 FP finding.

^{68}Ga-DOTA-TOC was FN in 2 patients. A 47-y-old woman was referred for initial staging of a NET unknown primary (patient 36). PET and SPECT were negative for multiple liver metastases that were histologically confirmed

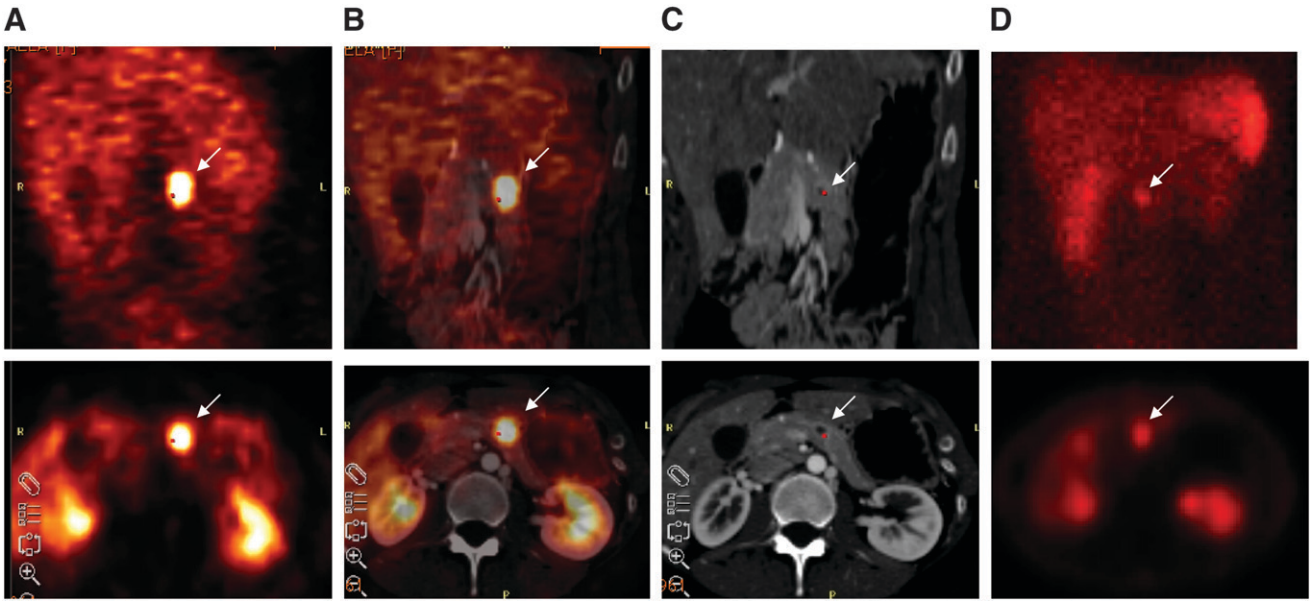

FIGURE 1. A 28-y-old female was referred for primary diagnosis of a NET because of elevated tumor markers in serum. PET (A) clearly depicted an abnormal focus in upper abdomen (arrow). This lesion could be delineated in the pancreas after image fusion with CT (B). There was also increased contrast medium enhancement in the margin when using helical CT (C). SPECT with ^{99m}Tc-HYNIC-TOC was also positive for this tumor in upper abdomen (D). This positive finding was confirmed by histopathology revealing a NET with 1 cm in diameter. (Top) Coronal views; (bottom) axial views.

by biopsy. Both nuclear medicine techniques were also negative for histologically confirmed small liver metastases in the other patient, a 67-y-old man (patient 78). This patient was referred for follow-up after surgery and chemotherapy of a rectal tumor. In both patients, diagnostic CT revealed a TP scan result.

^{68}Ga-DOTA-TOC and Functional Status of NET

The fraction of patients with clinical and biochemical features of a NET consisted of 18 TP, 8 TN, and 1 FP results, whereas in the group of patients with nonfunctioning tumors, 51 TP, 4 TN, and 2 FN results were observed. When comparing both groups, no statistically significant difference was found for PET ($P = 0.96$). Both patients with the FN scan result did not show any functional activity of the tumor, whereas the FP result was observed in a patient with elevated CgA level and persisting diarrhea, suggestive of a hormone-active tumor, as mentioned earlier.

PET Versus Scintigraphy (SPECT) and Diagnostic CT

All 3 modalities (PET, SPECT, and CT) showed an equivalent scan result in 39 patients (46.4%), including 27 TP and 12 TN results (Fig. 1).

Discrepancies between PET and SPECT were found in 32 patients (38%), all of whom were TP with PET and FN with SPECT. In this patient group, liver metastases were missed in 10 cases. Twenty-two additional small lymph node metastases also were not detected with SPECT in 15 patients. In 2 patients with carcinoid tumors, small peritoneal deposits escaped detection with SPECT. Furthermore, 32 bone metastases were not delineated by conventional scintigraphy but were positive with ^{68}Ga-DOTA-TOC PET. Discrepancies between PET and CT were found in 34 patients (40.5%), of whom there were 2 TP, 1 TN, 5 FP, and 26 FN findings with CT. FP findings with CT were caused by suggestive small nodular lung lesions in 2 patients and in 2 additional cases by enlarged lymph nodes. One 55-y-old male patient was referred for initial detection of a NET in the case of elevated CgA levels (patient 52). Abdominal

TABLE 3
SUVs at Different Time Points

Parameter	20 min	1 h	1 h 40 min
Liver	6.2 ± 1.7	5.9 ± 2.1	5.5 ± 2.4
Background	0.8 ± 0.5	0.6 ± 0.4	0.6 ± 0.4
Tumor in liver	12.9 ± 4.9	14.6 ± 5.9	15.8 ± 6.9
Tumor in abdomen	9.0 ± 6.7	10.6 ± 7.5	11.6 ± 7.2

SUV_{bw} is for selected tissue from 8 patients. SD gives interpatient variability.

TABLE 4
Results of PET vs. SPECT and CT: Analysis per Patient

		PET				SPECT				CT			
Group	*n*	TP	TN	FP	FN	TP	TN	FP	FN	TP	TN	FP	FN
Detection	13	4	8	1	0	2	8	1	2	3	8	1	1
Staging	36	32	3	0	1	14	3	0	19	16	3	2	15
Follow-up	34	33	1	0	1	21	1	0	13	22	1	2	10
Overall	84	69	12	1	2	37	12	1	34	41	12	5	26

TABLE 5
Comparison of 3 Imaging Modalities: PET, SPECT, and CT

Parameter	PET (%)	SPECT (%)	CT (%)
Sensitivity	97 (69/71)	52 (37/71)	61 (41/67)
Specificity	92 (12/13)	92 (12/13)	71 (12/17)
Accuracy	96 (81/84)	58 (49/84)	63 (53/84)

Number of patients is in parentheses.

TABLE 6
Site-Related Findings

Site	PET	SPECT	CT
Cranium	5	5	5
Neck/chest	35	30	31
Liver	56	46	56
Pancreas	23	21	19
Lymph nodes	90	68	87
Other	50	48	39
Bone	116	84	58
Overall	375	302	295

Other sites include, but are not mentioned, locations of tumor deposits—for example, peritoneal carcinosis.

CT visualized a lesion in the wall of the jejunum with a diameter of 1.4 cm. The contrast medium showed enhanced uptake of a primary NET. However, PET and SPECT were negative. Surgical exploration revealed a benign leiomyoma, which was proven by histology. Site-related differences are illustrated in Table 6.

Eighteen patients were investigated with both SPECT tracers, yielding a comparable scan result. The ^{99m}Tc-labeled compound was TP in 18 patients, TN in 11, FP in 1, and FN in 21 patients. When using ^{111}In-DOTA-TOC, the scan result was TP in 29 patients, TN in 1, and FN in 21 patients. No statistically significant difference was observed between the 2 groups ($P = 0.84$).

Clinically Valuable Information Obtained by PET

In 18 patients (21.4%), ^{68}Ga-DOTA-TOC provided further clinically relevant information in comparison with diagnostic CT alone, including 9 patients with unknown bone metastases (Fig. 2). The primary tumor or residual tumor at the primary site was demonstrated in 5 patients with ^{68}Ga-DOTA-TOC PET but escaped detection by CT. A 61-y-old woman (patient 65) was referred after treatment of a pulmonary carcinoid tumor for follow-up. Diagnostic CT was negative, but PET revealed small metastatic lesions in the myocardium and in the pancreas, with focally enhanced tracer accumulation. Multiple liver metastases were known in a 47-y-old woman (patient 80) who was investigated during follow-up after surgical resection of a small bowel carcinoid. ^{68}Ga-DOTA-TOC additionally showed a small lesion in the right breast initially not found with the other 2 modalities (Figure 3). This lesion with a diameter of 7–4 mm and 3 other metastases in the liver were surgically removed. In 2 patients, small liver metastases were not shown with diagnostic CT and SPECT (Fig. 4).

Compared with scintigraphy, ^{68}Ga-DOTA-TOC PET provided further valuable clinical information in 12 patients

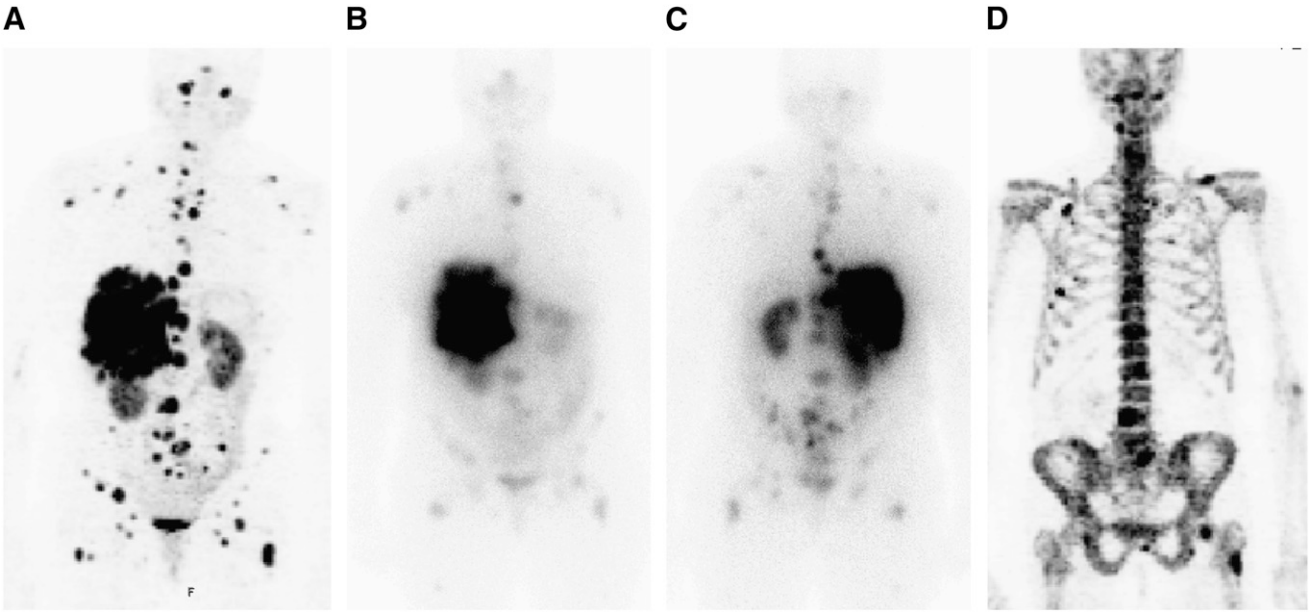

FIGURE 2. A 56-y-old woman with multiple liver and lymph node metastases was referred for restaging after surgery and chemotherapy. CT presented these tumor lesions; however, it was negative for bone lesions. Beside the visceral metastases, some additional osteoblastic and osteolytic bone metastases were clearly depicted with ^{68}Ga-DOTA-TOC (A). Only some of these bone metastases were delineated by conventional scintigraphy (B, anterior view; C, posterior view). Osteoblastic bone lesions were confirmed by ^{18}F-Na-fluoride PET (D). Retrospective CT analysis after image fusion revealed some of these bone metastases.

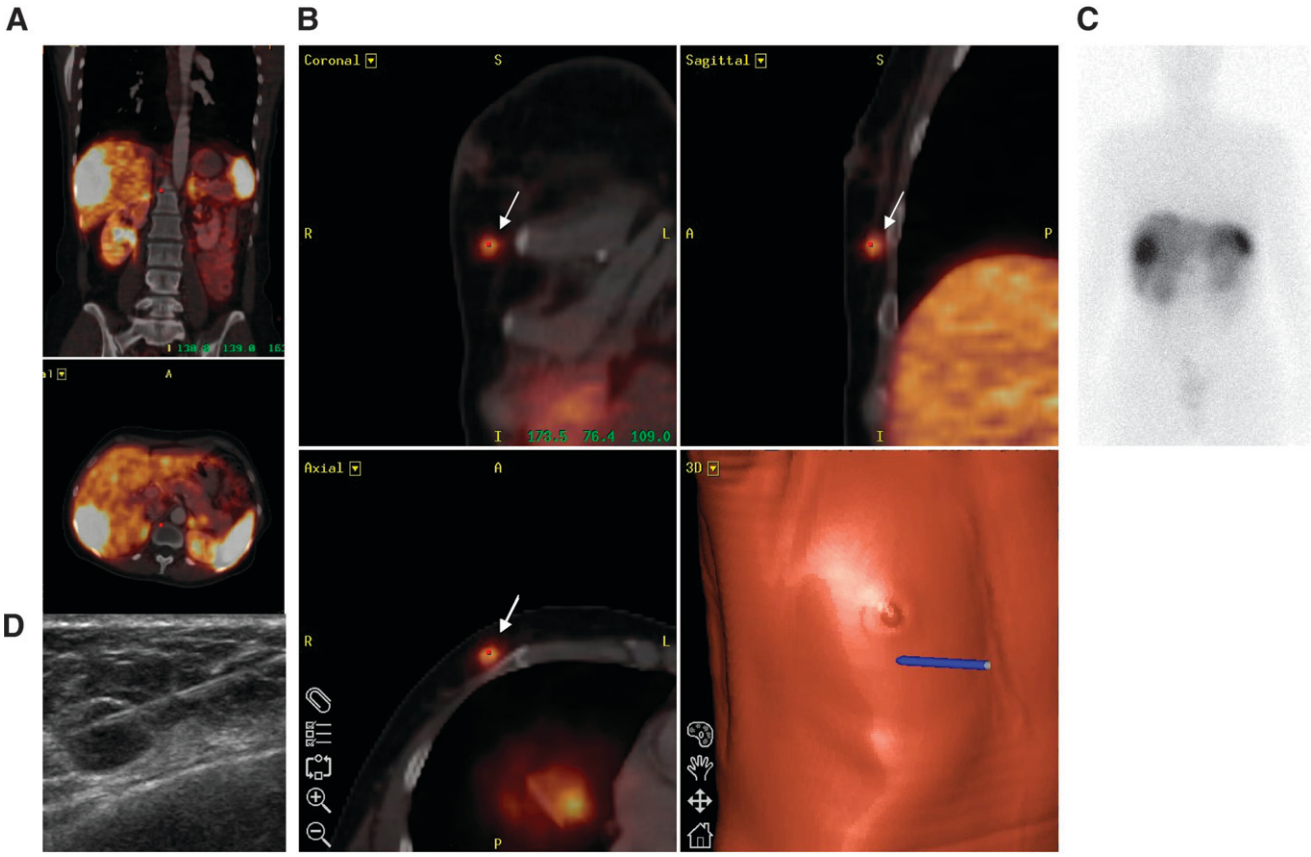

FIGURE 3. A 47-y-old female patient was referred for scanning after resection of a carcinoid of the ileum. Multiple liver metastases were known (A). Additionally, ^{68}Ga-DOTA-TOC showed a small lesion in right breast (arrows) (B). This finding was initially not detected with CT or scintigraphy (C). Ultrasound-guided fine-needle biopsy confirmed a metastasis in soft tissue derived from the NET with 7- to 4-mm diameter (D). This tumor lesion and 3 liver metastases were consecutively surgically removed.

(14.3%). Three patients have just been mentioned. Unknown bone metastases were shown in 5 patients. Surgical intervention was omitted in 3 patients because widespread disease was detected by ^{68}Ga-DOTA-TOC, showing additional unknown distant tumor lesions. One 34-y-old male patient was investigated after chemotherapy and chemoembolization of metastatic lesions in the liver of a NET unknown origin. PET additionally showed the primary tumor in the pancreatic head and local lymph node metastases (patient 34).

DISCUSSION

SRS has gained widespread acceptance as the imaging method of choice in NET patients, showing high sensitivity and good specificity for detection of the primary tumor and secondary lesions (*4,14,19–21*). However, because of low spatial resolution, this technique has a poor capability to detect lesions with smaller size and lower receptor density. ^{68}Ga-DOTA-TOC has emerged as a new PET tracer showing better results compared with conventional nuclear medicine examinations in a small group of patients (*12,13*). Initial results were confirmed by our prospective study in a larger number of patients with statistically significant higher diagnostic accuracy compared with conventional SRS as well as diagnostic CT. In 25% (21/84) of patients with NET, ^{68}Ga-DOTA-TOC provided additional information that was obtained with none of the other imaging procedures.

The better imaging properties are based on the higher spatial resolution of PET and on some beneficial pharmacokinetic properties of ^{68}Ga-DOTA-TOC (*22*) but also need an optimal acquisition protocol. Therefore, in 8 patients images were acquired at different times to evaluate the optimal time for acquisition, which turned out to be 100 min after injection by calculation of SUVs. SUVs were not used for diagnostic purposes, especially as the threshold and averaging method applied in this article is too complex for routine clinical use. Nevertheless, we do not rule out that simple maximum SUVs might be feasible as a clinical tool, taking into account our results.

The difference in detection rate was most pronounced for bone metastases–that is, of all 116 PET-positive lesions, SPECT delineated 84 (72.5%) lesions and CT delineated only 58 lesions (50%). These additional findings have prompted therapeutic interventions in some patients but also have a prognostic implication because unknown distant

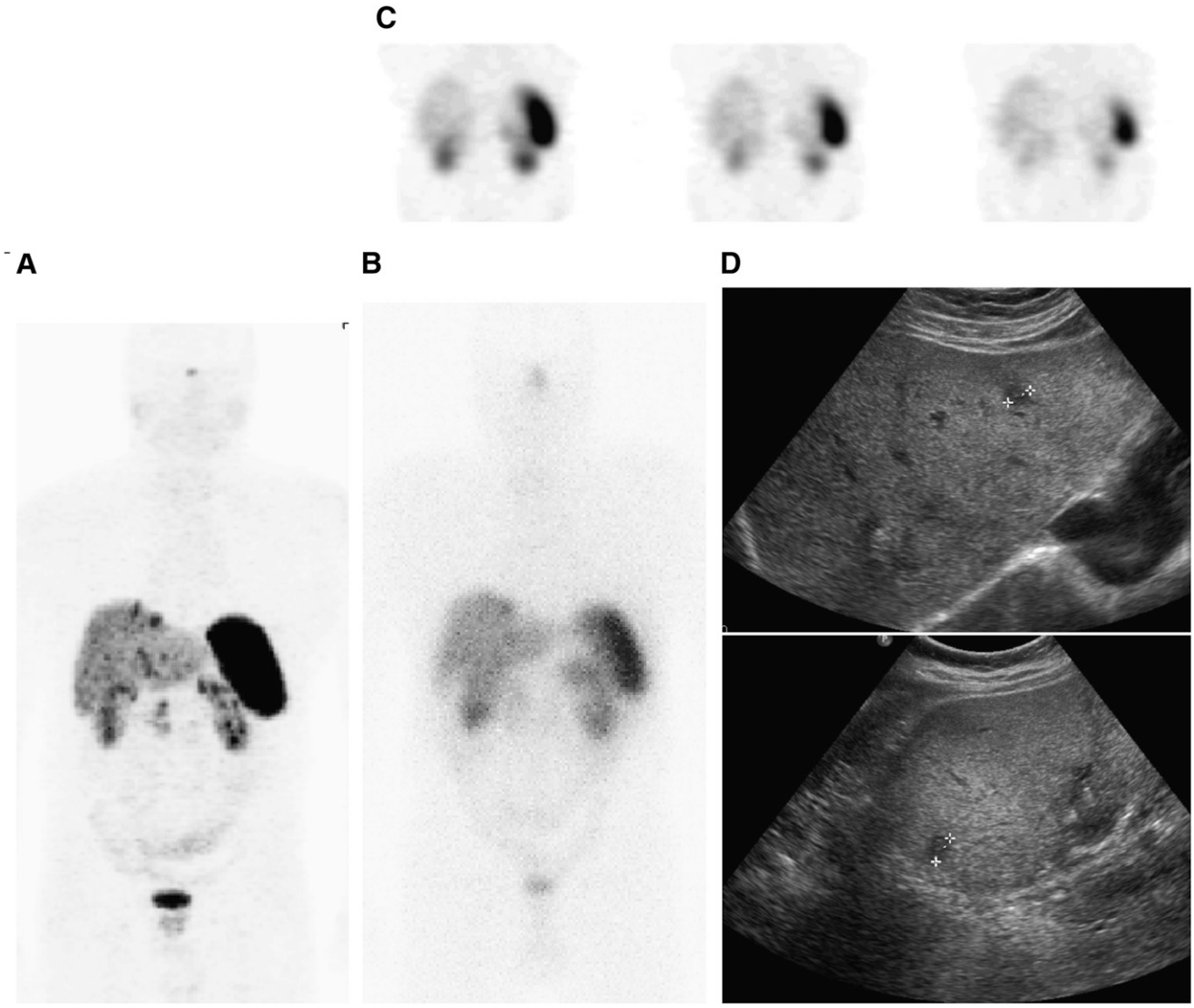

FIGURE 4. A 62-y-old male patient was investigated after resection of a small bowel carcinoid. ^{68}Ga-DOTA-TOC PET displayed multiple small liver metastases (A). These liver lesions were negative with the other 2 modalities, CT and scintigraphy (B) including SPECT (C). Ultrasonography (D) and further follow-up controls confirmed these lesions. Diameters of metastases were in the range of 1 cm. Positive PET finding initiated treatment with [^{177}Lu-DOTA^{0},Tyr^{3},Thr^{8}]octreotide (^{177}Lu-DOTA-TATE).

bone metastases are considered as a negative prognostic factor, possibly requiring a more aggressive treatment regime (*23,24*). On the other hand, some limitations can be found in the detection of liver metastases using ^{68}Ga-DOTA-TOC, as it is also known for SPECT (*7,8*). Radiologic techniques are found to be valuable for evaluation of this organ, in which metastases are frequently found in NET patients (*25,26*). In the present study the combined use of PET and CT also showed the highest overall accuracy for diagnosis of liver metastases, as CT provided complementary information in those 2 patients who were negative with PET. Diagnostic CT additionally reveals the individual anatomy, assisting in delineation of abnormal findings, which was very important in many patients when using ^{68}Ga-DOTA-TOC. On the other hand, tumor deposits—for example, bone metastases—frequently escaped detection by initial CT evaluation. Some of these lesions, however, were consecutively identified after image fusion in the CT scan guided by the findings of the PET scan. This implies that the PET scan is an excellent method for screening of tumor lesions followed by a more directed CT.

The very specific binding of ^{68}Ga-DOTA-TOC may lead to overinterpretation of tracer accumulation. Therefore, interpretation should be done cautiously in organs showing physiologically enhanced tracer uptake. The only FP case, for instance, was found in a patient with clinical features suggestive of a NET presenting focally enhanced tracer uptake in the pancreatic head mimicking the tumor.

One limitation of this study is based on the use of 2 different compounds for conventional scintigraphy, ^{99m}Tc-HYNIC-TOC and ^{111}In-DOTA-TOC. However, it has been shown for both radiopharmaceuticals that the detection

capability for NET is comparable with ^{111}In-DTPA-D-Phe^{1}-octreotide (where DTPA is diethylenetriaminepentaacetic acid) (*6,17,27*). Equivalent scan results were also obtained with both tracers in some patients, and no statistical difference was observed when ^{99m}Tc-HYNIC-TOC was compared with ^{111}In-DOTA-TOC. Therefore, conventional scintigraphy, including SPECT acquisition, was confined to 1 group for head-to-head comparison with PET.

^{11}C-5-Hydroxytryptophan and ^{18}F-fluoro-L-3,4-dihydroxyphenylalanine are substrates of the intermediary metabolic pathway in terms of the APUD concept (where APUD is amine precursor uptake and decarboxylation). Promising results have been obtained with both radiopharmaceuticals in patients with NET, exceeding the detection rate of SPECT and CT (*28,29*). A limitation of this concept seems to be that nonfunctioning tumors may be difficult to detect, as accumulation reflects the secretion pattern of peptide hormones (*28*). Furthermore, a decision on treatment using ^{90}Y-DOTA-TOC or [^{177}Lu-DOTA^{0},Tyr^{3},Thr^{8}]octreotide (^{177}Lu-DOTA-TATE) cannot be made on the basis of the uptake behavior in tumor lesions. In contrast, several patients were successfully treated with radiopeptide therapy because of a positive pretherapeutic scan result with ^{68}Ga-DOTA-TOC. With regard to patient convenience, it should be stressed that the whole investigation can be performed within 2 h, thereby creating lower radiation burden compared with some other nuclear medicine techniques as indicated by preclinical (*30*) and clinical studies (*12,13*).

The use of a generator for a short-lived radionuclide such as ^{68}Ga provides the basis for convenient, easy use of this radionuclide. Labeling of DOTA-derivatized peptides is straightforward and can be performed in a very short time (<30 min). This guarantees a high flexibility and good availability of this radiopharmaceutical in clinical routine in contrast to ^{11}C-labeled compounds, requiring access to an on-site cyclotron unit, or some ^{18}F-labeled derivatives, such as *N*-(1-deoxy-D-fructosyl)-*N*-(2-^{18}F-fluoroproionyl)-Lys^{0},Tyr^{3}-octreotate (Gluc-Lys(^{18}F-FP)-TOCA) (*31*), requiring multistep synthesis with several purification steps.

CONCLUSION

Somatostatin receptor PET with ^{68}Ga-DOTA-TOC is superior for the detection of NET compared with SPECT and diagnostic CT in various clinical situations (initial diagnosis, staging, and follow-up). The higher sensitivity for tumor detection has clinical impact in a considerable number of patients, especially when compared with CT. However, the best results are to be achieved by the combination of PET and CT. It also indicates receptor expression for targeted radiopeptide therapy.

REFERENCES

1. Reubi JC. Peptide receptors as molecular targets for cancer diagnosis and therapy. *Endocr Rev.* 2003;24:389–427.
2. Quaedvlieg PF, Visser O, Lamers CB, Janssen-Heijen ML, Taal BG. Epidemiology and survival in patients with carcinoid disease in The Netherlands: an epidemiological study with 2,391 patients. *Ann Oncol.* 2001;12:1295–1300.
3. Modlin IM, Lye KD, Kidd M. A 5-decade analysis of 13,715 carcinoid tumors. *Cancer.* 2003;97:934–959.
4. Krenning EP, Kwekkeboom DJ, Bakker WH, et al. Somatostatin receptor scintigraphy with [^{111}In-DTPA-D-Phe^{1}]- and [^{123}I-Tyr^{3}]-octreotide: the Rotterdam experience with more than 1000 patients. *Eur J Nucl Med.* 1993;20:716–731.
5. Seregni E, Chiti A, Bombardieri E. Radionuclide imaging of neuroendocrine tumors: biological basis and diagnostic results. *Eur J Nucl Med.* 1998;25:639–658.
6. Gabriel M, Decristoforo C, Donnemiller E, et al. An intrapatient comparison of ^{99m}Tc-EDDA/HYNIC-TOC with ^{111}In-DTPA-octreotide for diagnosis of somatostatin receptor expressing tumors. *J Nucl Med.* 2003;44:708–716.
7. Gabriel M, Muehllechner P, Decristoforo C, et al. ^{99m}Tc-EDDA/HYNIC-Tyr^{3}-octreotide for staging and follow-up of patients with neuroendocrine gastroentero-pancreatic tumors. *Q J Nucl Med Mol Imaging.* 2005;49:237–244.
8. Dromain C, de Baere T, Lumbroso J, et al. Detection of liver metastases from endocrine tumors: a prospective comparison of somatostatin receptor scintigraphy, computed tomography, and magnetic resonance imaging. *J Clin Oncol.* 2005;23:70–78.
9. Adams S, Baum R, Rink T, Schumm-Drager PM, Usadel KH, Hor G. Limited value of fluorine-18 fluorodeoxyglucose PET for the imaging of neuroendocrine tumors. *Eur J Nucl Med.* 1998;25:79–83.
10. Horton KM, Fishman EK. The current status of multidetector row CT and three-dimensional imaging of the small bowel. *Radiol Clin North Am.* 2003;41:199–212.
11. Gabriel M, Hausler F, Bale R, et al. Image fusion analysis of ^{99m}Tc-HYNIC-Tyr^{3}-octreotide SPECT and diagnostic CT using an immobilization device with external markers in patients with endocrine tumours. *Eur J Nucl Med Mol Imaging.* 2005;32:1440–1451.
12. Hofmann M, Maecke H, Borner R, et al. Biokinetics and imaging with somatostatin receptor PET radioligand ^{68}Ga-DOTATOC: preliminary data. *Eur J Nucl Med.* 2001;28:1751–1757.
13. Kowalski J, Henze M, Schuhmacher J, Maecke HR, Hofmann M, Haberkorn U. Evaluation of positron emission tomography imaging using [^{68}Ga]-DOTA-D-Phe^{1}-Tyr^{3}-octreotide in comparison to [^{111}In]-DTPAOC SPECT: first results in patients with neuroendocrine tumors. *Mol Imaging Biol.* 2003;5:42–48.
14. Balon HR, Goldsmith SJ, Siegel BA, et al. Procedure guideline for somatostatin receptor scintigraphy with ^{111}In-pentetreotide. *J Nucl Med.* 2001;42:1134–1138.
15. Breeman WA, de Jong M, de Blois E, Bernard BF, Konijnenberg M, Krenning EP. Radiolabelling DOTA-peptides with ^{68}Ga. *Eur J Nucl Med Mol Imaging.* 2005;32:478–485.
16. Guggenberg E, Mikolajczak R, Janota B, Riccabona G, Decristoforo C. Radiopharmaceutical development of a freeze-dried kit formulation for the preparation of [^{99m}Tc-EDDA-HYNIC-D-Phe1,Tyr3]-octreotide, a somatostatin analog for tumor diagnosis. *J Pharm Sci.* 2004;93:2497–2506.
17. de Jong M, Bakker W, Krenning E, et al. Yttrium-90 and indium-111 labelling, receptor binding and biodistribution of [DOTA^{0},D-Phe^{1},Tyr^{3}]octreotide, a promising somatostatin analogue for radionuclide therapy. *Eur J Nucl Med.* 1997;24:368–371.
18. Debray MP, Geoffroy O, Laissy JP, et al. Imaging appearance of metastases from neuroendocrine tumours of the pancreas. *Br J Radiol.* 2001;74:1065–1070.
19. Krenning EP, Kwekkeboom DJ, de Jong M, et al. Essentials of peptide receptor scintigraphy with emphasis on somatostatin analog octreotide. *Semin Oncol.* 1994;21(suppl 13):6–14.
20. Lamberts SWJ, Reubi JC, Krenning EP. Somatostatin and the concept of peptide receptor scintigraphy in oncology. *Semin Oncol.* 1994;21(suppl 13):1–5.
21. Kwekkeboom D, Krenning EP, de Jong M. Peptide receptor imaging and therapy. *J Nucl Med.* 2000;41:1704–1713.
22. Heppeler A, Froidevaux S, Eberle A, Maecke H. Receptor targeting for tumor localisation and therapy with radiopeptides. *Curr Med Chem.* 2000;7:971–994.
23. Panzuto F, Nasoni S, Falconi M, et al. Prognostic factors and survival in endocrine tumor patients: comparison between gastrointestinal and pancreatic localization. *Endocr Relat Cancer.* 2005;12:1083–1092.
24. Gupta S, Johnson MM, Murthy R, et al. Hepatic arterial embolization and chemoembolization for the treatment of patients with metastatic neuroendocrine tumors: variables affecting response rates and survival. *Cancer.* 2005;104:1590–1602.
25. Kumbasar B, Kamel IR, Tekes A, Eng J, Fishman EK, Wahl RL. Imaging of neuroendocrine tumors: accuracy of helical CT versus SRS. *Abdom Imaging.* 2004;29:696–702.
26. Schillaci O, Spanu A, Scopinaro F, et al. Somatostatin receptor scintigraphy with ^{111}In-pentetreotide in non-functioning gastroenteropancreatic neuroendocrine tumors. *Int J Oncol.* 2003;23:1687–1695.

27. Kwekkeboom DJ, Kooij PP, Bakker WH, Maecke HR, Krenning EP. Comparison of ^{111}In-DOTA-Tyr^{3}-octreotide and ^{111}In-DTPA-octreotide in the same patients: biodistribution, kinetics, organ and tumor uptake. *J Nucl Med.* 1999;40:762–767.
28. Orlefors H, Sundin A, Garske U, et al. Whole-body ^{11}C-5-hydroxytryptophan positron emission tomography as a universal imaging technique for neuroendocrine tumors: comparison with somatostatin receptor scintigraphy and computed tomography. *J Clin Endocrinol Metab.* 2005;90:3392–3400.
29. Becherer A, Szabo M, Karanikas G, et al. Imaging of advanced neuroendocrine tumors with ^{18}F-FDOPA PET. *J Nucl Med.* 2004;45:1161–1167.
30. Ugur O, Kothari PJ, Finn RD, et al. Ga-66 labeled somatostatin analogue DOTA-DPhe^{1}-Tyr^{3}-octreotide as a potential agent for positron emission tomography imaging and receptor mediated internal radiotherapy of somatostatin receptor positive tumors. *Nucl Med Biol.* 2002;29:147–157.
31. Meisetschlager G, Stahl A, et al. Gluc-Lys([^{18}F]FP)-TOCA PET in patients with SSTR-positive tumors: biodistribution and diagnostic evaluation compared with [^{111}In]DTPA-octreotide. *J Nucl Med.* 2006;47:566–573.